FIRE AND MATERIALS
Fire Mater. 2016
Published online in Wiley Online Library (wileyonlinelibrary.com). DOI: 10.1002/fam.2375

Hexaphenoxycyclotriphosphazene as FR for CFR anionic PA6 via T-RTM: a study of mechanical and thermal properties

Carl-Christoph Höhne[1,2,*,†], Rainer Wendel[1,*], Bert Käbisch[1,2,*], Thorsten Anders[1], Frank Henning[1,3] and Edwin Kroke[2]

[1] *Fraunhofer Institut für Chemische Technologie, Pfinztal 76327, Germany*
[2] *Institut für Anorganische Chemie, Technische Universität Bergakademie Freiberg, Freiberg 09596, Germany*
[3] *Karlsruher Institut für Technologie (KIT), Institut für Fahrzeugsystemtechnik, Karlsruhe 76131, Germany*

SUMMARY

The production of carbon fiber reinforced (CFR) anionic polyamide 6 (APA6) plates by thermoplastic resin transfer molding (T-RTM) processing is highly sensitive to the presence of polymer additives such as flame retardants (FRs). However, APA6 is flammable, and therefore, it is mandatory to protect the polymer matrix, especially if the produced materials are intended for aerospace applications. Typically used FR for PA6 cannot be incorporated in the T-RTM processes. With hexaphenoxycyclotriphosphazene, an incorporable and effective FR additive for CFR APA6 was discovered. Cone calorimetry measurements indicate a char formation-based mechanism, and the flame retardancy was further confirmed with limiting oxygen index tests, classification by UL94 (V-0), and FAR25 tests. The influence of this FR on the thermal (thermogravimetric analysis and differential scanning calorimetry) and mechanical behavior (flexural, compressive and ultimate tensile strength, and Charpy impact tests) on CFR APA6 produced via T-RTM processing is evaluated and indicates no interaction with the APA6; it works as a passive filler. Copyright © 2016 John Wiley & Sons, Ltd.

Received 6 October 2015; Revised 26 April 2016; Accepted 4 May 2016

KEY WORDS: anionic polyamide 6 (APA6); cast polyamide 6 (cast PA6); carbon fiber reinforced plastics; thermoplastic resin transfer molding (T-RTM); flame retardant; nitrogen; phosphorous; phosphazene

1. INTRODUCTION

Lightweight constructions produced from reinforced polymeric materials are essential for aerospace construction because of the large economic and ecological benefits of weight saving [1]. Nowadays, thermoset and thermoplastic composites, particularly carbon fiber reinforced (CFR) thermosets, take the biggest part of the structural mass of an aircraft [2, 3]. Thermosets, especially CFR epoxy resins, are often used because of high stiffness and strength [2]. CFR thermoplastics do not show the same strength as CFR thermosets, but they have unlimited shelf life (avoid material age and storage problems), wide range and simpler manufacturing, short processing time (chemical curing is not needed), ability to be re-formed, high chemical resistance, low water absorption, and improved impact resistance [2,4]. Furthermore, they are repairable [4] or recyclable [5] by remelting of the thermoplastic matrix. Therefore, thermoplastics are interesting matrix polymers for the investigation of new cost-efficient aerospace materials. In this paper, we investigate the thermoplastic polymer

*Correspondence to: Carl-Christoph Höhne, Bert Käbisch, Institut für Anorganische Chemie, Technische Universität Bergakademie Freiberg, Freiberg 09596, Germany; and Rainer Wendel, Fraunhofer Institut für Chemische Technologie, Pfinztal 76327, Germany.
†E-mail: carl-christoph.hoehne@ict.fraunhofer.de; Bert.Kaebisch@ict.fraunhofer.de; Rainer.Wendel@ict.fraunhofer.de

polyamide 6 (PA6) as a material for CFR aircraft panels. To fabricate CFR PA6 plates, we used anionic polymerized PA6 (APA6) produced by thermoplastic resin transfer molding (T-RTM) processing.

The resin transfer molding (RTM) process to produce CFR plastics is known for resins with low application viscosity, for example, epoxy and vinyl esters [6, 7]. Thermoplastics are usually unsuitable in RTM processes because of high melt viscosity [7]. However, CFR plastic with a thermoplastic PA6 matrix can be produced by the injection of ε-caprolactam via RTM, followed by an anionic ε-caprolactam polymerization to produce APA6 [8] in a so-called T-RTM process [7]. For example, Volkswagen AG, BASF SE, and KraussMaffei Technologies built a B-pillar prototype consisting of glass fiber (GF)-reinforced APA6 by T-RTM processing [7].

For aerospace materials, particularly for materials used in passenger cabins, fire protection is in addition to mechanical properties one of the most essential material characteristics. It is well known that PA6 is a flammable material [9]. In order to meet fire resistance standards in an aircraft application, CFR APA6 systems require utilization of flame retardants (FRs) in addition to the inflammable reinforcement. Typical FRs used to protect PA6 are halogenated FRs, triazine derivates, such as melamine or melamine polyphosphate, mineral fillers like magnesium hydroxide or silicate minerals, and phosphorus compounds, including red phosphorus, alkylphosphonate, or phosphorus oxynitride [9–20]. However, most of them are not applicable via T-RTM processing because their incorporation has a negative impact on the course of anionic polymerization. Additionally, these FRs are typically not soluble in the monomer melt, and the fiber fabric separates them from the molten ε-caprolactam during the T-RTM processing. Consequently, the aim of this work was the development of an effective FR system for CFR APA6, which is incorporable via T-RTM processing. We found that out of twelve commonly used FRs for PA6, only the hexaphenoxycyclotriphosphazene (HPCPT)-based FR Rabitle® FP110 (FP110) is able to be incorporated in the T-RTM process and to protect CFR APA6.

Phosphazenes are cyclic (cyclo-) or polymeric (poly-) molecules consisting of alternating phosphorus and nitrogen atoms [21]. Since there first description in 1834 by Wöhler and Liebig [22] and by Rose [23] and the beginning of modern polyphosphazene chemistry, essentially initiated by Allcock, Kugel, and Valan [24–26], many phosphazene derivates and phosphazene applications have been developed [27]. With more than 700 polymers of very diverse properties [28–35], polyphosphazenes are one of the biggest groups of inorganic polymers [36]. Flame retardancy of phosphazenes is the oldest and most continuously advanced application [37], especially the FR efficiency of cyclophosphazene additives, which was proven in many polymer systems like polyurethane, polystyrene, epoxy, and others [10,17,37–57]. Also for PA6 and PA6,6, it is known that cyclophosphazenes can be used as FRs, while HPCPT is the most popular one [10,13,58–66]. For example, V-2 till V-0 UL94 classifications are reported for PA6,6 with 25% GF and a FR combination of HPCPT, aluminum diethylphosphinate, and melamine polyphosphate or HPCPT and red phosphorous [59–62]. For PA6 with 30% GF and 10% polyphenylethers, V-2 classifications are reported for 15% HPCTP and V-0 classification with the addition of zinc borate [64, 65].

2. EXPERIMENTAL PROCEDURES

2.1. Materials

For the FR investigations, Rabitle FP110 (Fushimi Pharmaceutical Co Ltd.; supplier: Nordmann, Rassmann), Aflammit PCO 960 (THOR), Exolit OP 935, OP 1312 and AP 462 (Clariant), Apyral 40 CD and 40 VS1 (NabalTec), melamine (Sigma-Aldrich), expendable graphite (Naturgraphit AG), Magnifin H5 IV (Albemarle) red phosphorus (ItalMatch), and methyl-DOPO (FhG-ICT [67]) are used. The CFR APA6 plates are prepared using the following materials: ε-caprolactam from Lanxess, APA6-catalyst Brüggolen C10, APA6-activator Brüggolen C20P from Brüggemann Chemical, and a carbon fiber fleece UD #030-1 with parallel fiber orientation from Engineered Cramer Composites. The release agent for the mold is PAT-626 from Würtz. All materials are used without further purification.

DOI: 10.1002/fam

2.2. *Preparation of APA6 and CFR APA6 plates*

The CFR APA6 plates ($650 \times 480 \times 2\,mm^3$) are manufactured via T-RTM processing using a plate mold and a low pressure injection equipment. For manufacturing ε-caprolactam separately with 2 wt % of APA6-activator Brüggolen C20P, ε-caprolactam with 4 wt% of APA6-catalyst Brüggolen C10 and FP110 (dried in vacuum for 3 days at 60 °C) are molten at 110 °C in the dosing unit. Both melts are mixed in a ratio of 1:1 and injected from one side into the mold. The cavity of the mold is 2.2 mm. The injection quantities are $800\,cm^3$ for productions without carbon fabric and $670\,cm^3$ for productions with carbon fabric reinforcement by a flow rate of $40.9\,cm^3/s$. For production of reinforced plates, seven carbon fabric layers are placed inside the mold prior to injection of the melt. The polymerization process is carried out for 360 s at 150 °C. After the polymerization, the plates are dried for 3 days at 70 °C according to DIN EN ISO 1110 (Figure 1).

2.3. *Characterization*

2.3.1. Cone calorimetry. The measurements were conducted on a cone calorimeter from FTT Fire Testing Technology Ltd. (East Grinstead, UK) using the ISO 5660-1 standard. All samples were conditioned for 24 h at 23 °C and 50% relative humidity and were tested with $50\,kW/m^2$ heat flux. A sample size of $100 \times 100 \times 2\,mm^3$ was chosen. The CO and CO_2 calibration was carried out in vol. %. The presented data of each sample set are averages of two measurements.

2.3.2. Thermogravimetric analysis. The measurements were performed with a TGA Q5000 from TA Instruments. The heating rate was 5 K/min. Nitrogen and synthetic air (80% nitrogen + 20% oxygen) were used as atmospheres. The sample mass was between 1 and 10 mg.

2.3.3. Limiting oxygen index test. The limiting oxygen index (LOI) value was measured using an oxygen index module from FIRE on sheets measuring $7 \times 6.5 \times 3\,mm^3$ according to DIN EN ISO 4589-2 standardized procedure.

2.3.4. UL94 test. The UL94 tests were performed with a UL94 Test Device from WAZAU, Germany, according to DIN EN 60695-11-10 and DIN EN 60695-11-20 norms (sample size: $127 \times 13 \times 2\,mm^3$).

2.3.5. FAR 25.853 test. The Federal Aviation Regulations (FAR) tests were conducted using the UL94 Test Device from WAZAU, Germany, according to FAR, part 25.853, appendix F1, (a)(1)(i).

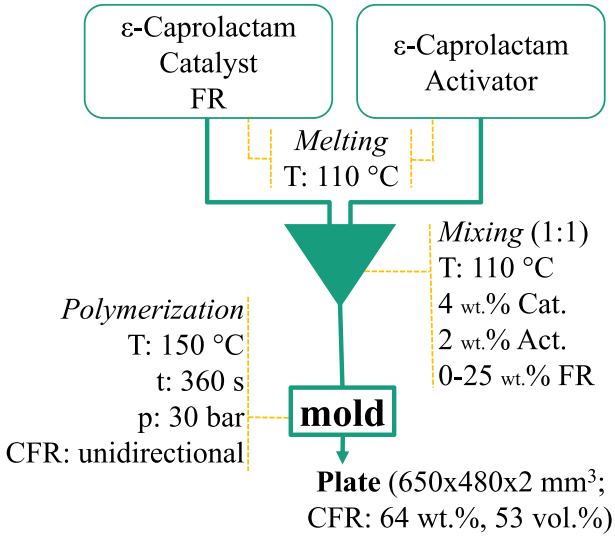

Figure 1. Flowchart of the thermoplastic resin transfer molding process.

DOI: 10.1002/fam

2.3.6. Fiber content measurement. The fiber content was measured using a thermogravimetric analysis (TGA) technique. Each sample was pyrolyzed at 650 °C for 50 min in a nitrogen atmosphere. The testing machine was TGA701 from Leco.

2.3.7. Residual monomer measurement. The residual monomer was extracted with water and measured with a HPLC laboratory device Agilent 1100 Series.

2.3.8. Flexural test. For the measurements, an inspekt table 5 kN tester from Hegewald & Peschke (three-point flexural test technique) with a 5 kN-measuring box and a test speed of 5.5 mm/min was used. The sample size was $25 \times 2\,mm^2$ with a pad distance of 82 mm. All samples were conditioned for 24 h at 23 °C and 50% relative humidity and were tested by 0° fiber orientation according to DIN 14125.

2.3.9. Compressive test. The measurements were performed with a universal testing machine 100 kN from Zwick according to DIN EN ISO 14126 norm. The sample size was $10 \times 2\,mm^2$ (B1 according to DIN EN ISO 14126:1999). All samples were conditioned for 24 h at 23 °C and 50% relative humidity and were tested by 0° and 90° fiber orientation.

2.3.10. Tensile test. For the measurements, an inspekt table 50 kN tester (Hegewald & Peschke) with a 50 kN-measuring box or an inspekt 250 kN (Hegewald & Peschke) with a 250 kN-measuring box and a test speed of 1 mm/min were used. The tests were carried out according to DIN EN ISO 527-1 standard. The samples measuring $25 \times 2\,mm^2$ were conditioned for 24 h at 23 °C and 50% relative humidity and were tested with a 0° and 90° fiber orientation.

2.3.11. Impact resistant test. The measurements were carried out by a RESIL Impactor according to the Charpy ISO 176-1/1fU procedure. The sample size was $10 \times 2\,mm^2$ with a pad distance of 41 mm. All samples were conditioned for 24 h at 23 °C and 50% relative humidity and were tested with a 0° fiber orientation.

2.3.12. Differential scanning calorimetry. The measurements were performed with a DSC Q2000 from TA Instruments. The heating rate was 10 K/min, and nitrogen was used as atmosphere. Each sample was heated up to 250 °C, subsequently cooled down to 0 °C, and heated up again till 250 °C. The sample mass was between 6 and 10 mg.

3. RESULTS AND DISCUSSION

Some disadvantages exist for the use of CFR thermoplastics in aerospace applications; by name, high process temperatures and high process pressures are required, and raw materials are expensive because polyetheretherketone (PEEK) and polyphenylenesulfide (PPS) are probably the most widely used high performance thermoplastic resins [4]. To overcome these disadvantages, we investigate CFR APA6 produced by the following four reasons:

1. Low viscosity of ε-caprolactam

Polyamide 6-based structures can be produced by remelting of PA6 (usually formed by hydrolytic lactam polymerization) or by an *in-situ* anionic polymerization [8]. To produce APA6, molten ε-caprolactam is polymerized in an anionic ring opening reaction, induced usually by a basic catalyst, for example, sodium salt of ε-caprolactam, directly in the mold [8]. Because of the much lower viscosity of ε-caprolactam compared with PA6, molds of complex design can be fulfilling easier [68], and of particular importance is that fiber fabrics for fiber reinforcements are easier to be infiltrated. Consequently, for the production of CFR PA6 with high fiber content via T-RTM processing, APA6 should produce better material properties because of good fiber infiltration [69, 70].

2. Low process temperatures

The remelt process of PA6 (mp: approx. 223 °C) needs temperatures around 250–270 °C [8]. However, the APA6 polymerization (ε-caprolactam mp: approx. 70 °C) is carried out at 140–180 °C in addition of a cocatalyst (activator), for example, an isocyanate [5,8]. Consequently, energy costs should be lower in case of APA6.

DOI: 10.1002/fam

Table I. Results of the FRs tested in CFR APA6.

No.	FR	Soluble in molten ε-caprolactam	Polymerizable
1	Rabitle FP110[a]	Yes (tested: till 50 wt%)	Yes
2	Aflammit PCO 960	Yes (tested: till 10 wt%)	Yes (till 1 wt%)
3	Methyl-DOPO	Yes (tested: till 10 wt%)	Yes (till 5 wt%)
4	Melamine	No	No
5	Expandable graphite	No	No
6	Exolit OP 935	No	No
7	Exolit OP 1312	No	No
8	Exolit AP 462	No	Yes
9	Apyral 40 CD	No	Yes
10	Apyral 40 VS1	No	Yes
11	Magnesium hydroxide (Magnifin H5 IV)	No	Yes
12	Red phosphorus	No	Yes

[a]Rabitle FP110 is a HPCPT-based FR (approx. 80% HPCPT and 20% phenoxycyclotetra till phenoxycyclooctaphosphazene (i.e. the larger phosphazene rings); Y. Tada, Fushimi Pharmaceutical).

3. High crystallinity of APA6

Crystallinity is one of the important characteristics of a high-performance polymer [4]. High crystallinity causes high stiffness and high tensile strength (amorphous regions adsorbing impact energy better) [4]. Consequently, APA6 is more appropriated to produce high-performance PA6 as hydrolytically polymerized PA6 because molecular mass and crystallinity of APA6 are higher [8].

4. Low process costs

Polyamide 6 is the most commonly used type of polyamides and because of this, ε-caprolactam is a cheap material particularly in comparison to PEEK or PPS (sales price ratios [71] (nylon: high-temperature polymers like PEEK and PPS) = 1:3 to 1:20). Also, the manufacturing process is cheap because only minutes are needed for the anionic polymerization of ε-caprolactam [8].

3.1. Flame retardancy

Several commercially available FRs were tested for an application via T-RTM processing. A summary of the obtained results is presented in Table I.

Nine of the twelve tested FRs were insoluble in molten ε-caprolactam, and therefore, filtered out by the carbon fibers. Three of the examined FRs were soluble in the molten matrix, but only Rabitle FP110 did not interrupt the polymerization process and showed the required properties for the T-RTM process: melt during ε-caprolactam melting, no interaction with the anionic ε-caprolactam polymerization, and good compatibility up to 25 wt%[‡]. An explanation for this result could be the steric shielding of the phenoxy groups of HPCPT. The nucleophilic phosphorus atoms of Aflammit PCO 960 and Methyl-DOPO are easily accessible for a reaction with the catalyst or the reactive anionic polymer chain. The nucleophilic phosphorus atoms of the phosphazene core in HPCPT are hard to access because of the six phenoxy groups. An interaction and interruption of the anionic polymerization of ε-caprolactam is obviously not possible.

3.1.1. Cone calorimetry. The results of the cone calorimeter measurements by means of the time to ignition (t_{ig}), peak heat release rate (HRR), total heat release (THR), total heat evolved, total smoke release (TSR), burning time (t_b), maximal average rate of heat emission, and the concentration of CO and CO_2 are discussed. Table II shows the data obtained during the experiments, while the HRR and THR curves of CFR APA6 are shown in Figure 2.

Four clear tendencies can be identified based on Figure 2:

[‡]In all cases, the FP110 content was calculated based on the polymer matrix mass without the reinforcing fiber fabric mass.

DOI: 10.1002/fam

Table II. Cone calorimetry results for CFR APA6 plates ($100 \times 100 \times 2\,mm^3$).

FP110 [wt%]	t_{ig} [s]	Peak HRR [kW/m^2]	THE [MJ/m^2]	TSR [m^2/m^2]	t_b [s]	MARHE [kW/m^{2}s]
0	43	195	36.1	60.1	513	125.9
	50	201	35.1	128.2	557	126.5
5	44	174	28.1	389.2	455	114.8
	44	177	30.4	418.7	444	117.5
10	38	154	24.6	528.5	314	105.5
	41	156	25.9	526.9	390	105.7
15	50	150	23.8	522.9	384	96.6
	43	146	23.0	528.2	433	98.3
25	50	147	21.0	682.8	336	88.4
	57	152	17.8	624.9	423	85.4

(a) t_{ig}, time to ignition; (b) HRR, heat release rate; (c) THE, total heat evolved; (d) TSR, total smoke release. (e) t_b, burning time; (f) MARHE, maximal average rate of heat emission.

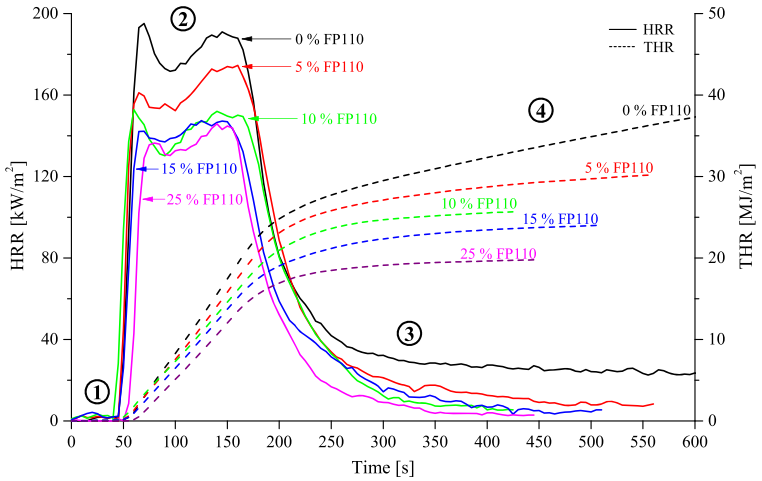

Figure 2. Heat release rate (line) and total heat release (dashed line) curves of carbon fiber reinforced (CFR) anionic polyamide 6 (APA6).

1. *Ignition*: All t_{ig} averages were in the same range between 40 and 47 s except for the sample containing 25 wt% of FP110, which showed slightly delayed ignition after 54 s probably caused by incipient charring and dilution of APA6 volume fraction by FP110.
2. *Burning*: With increasing FR load, the HRR and the t_b decreased (Table II). The observed HRR curves (double peak) are typical for thermally thick charring materials [72]. The lowest peak HRRs, observed for 15 and 25 wt% FP110, are around 149 k Wm^{-2}.
3. *After the burn*: The HRR of all FP110 containing samples tended to zero (slower for samples with lower FP110 loading). But pure CFR APA6 showed a constant HRR until the end of measurement caused by after glowing.
4. *THR*: The THR decreased with increasing FP110 load. Total heat evolved (THR at the end of burning time) is nearly by a factor of two lower at 25 wt% FP110 in comparison with pure CFR APA6.

The investigation of the gas phase environments produced by burning samples shows also a high influence of the FR. An increasing FP110 load increases the total smoke release (TSR, Table II). Even with 5 wt% FP110, the average TSR grows more than fourfold, and with 25 wt% FP110, the value is nearly seven times increased relative to pure CFR APA6. Figure 3 displays the CO_2 and CO proportion in the gas phase. The amount of emerging CO rises with higher FP110 loads, whereas the CO_2 amount is lowered.

The mass loss during the cone calorimetry is presented in Figure 4. Until 240 s, all samples, also with 5 and 10 wt% FP110, show the same tendency (deviation from FP110 free sample is less than 2 wt%) — nearly constant weight until time of ignition and subsequent continuous mass loss. After

DOI: 10.1002/fam

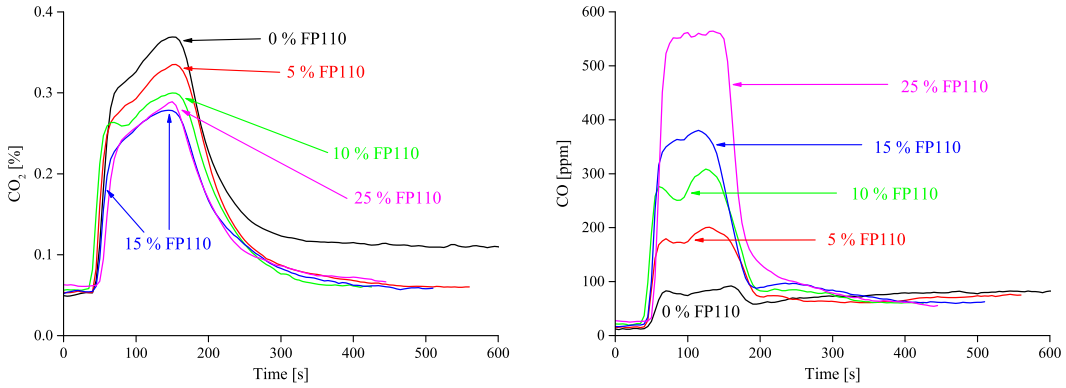

Figure 3. CO_2 and CO release of CFR APA6.

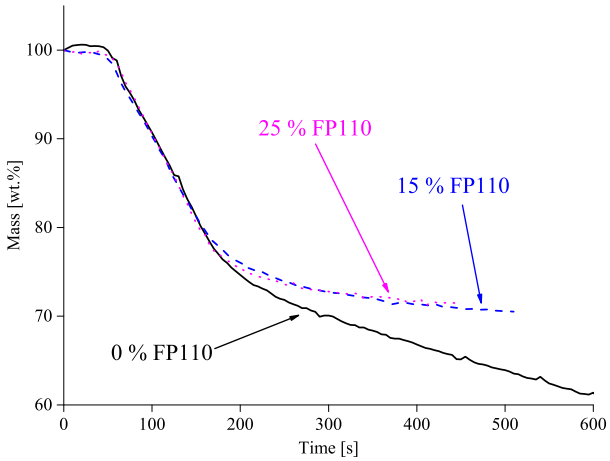

Figure 4. Mass loss during the cone calorimetry of CFR APA6.

more than 240 s, the mass of pure APA6 decreases continually as a result of afterglow, while the residue mass of the flame retardant samples is around 69 wt%. The differences of residual mass between the 5 and 25 wt% FP110 samples are in the area of 1.5 wt%.

All cone calorimetry results lead to two main effects of the FR FP110. On the one hand, FP110 dilutes the burnable polymeric material, whereby HRR decreases after ignition. At the same time, a fire-protecting char is formed through the FR solid phase action. According to the measured mass losses (Figure 4), the char cannot extinguish the fire – the mass losses in the main fire period at the first 200 s are nearly the same – but the sample afterglow is prevented. On the other hand, higher smoke release and CO proportions are detected in presence of the FR. A reason for this is perhaps a flame inhibiting effect in the gas phase. It is also possible that FP110 act as an oxygen limiter by the formation of P-O or N–O bonds, whereby the CO amount rises. These two mechanisms, lower oxygen amount on the polymeric surface and additionally a radical scavenger effect, lead to an incomplete combustion and oxidation of the polymeric matrix. Consequently, the smoke release grows. Furthermore, the char-forming process of hexaphenoxycyclotriphosphazene, a thermal cross-linking reaction by an electrophilic aromatic substitution reaction between the phosphazene core and the phenoxy group during the release of phenol [73] in the gas phase, can also cause an intensive smoke production.

3.1.2. Thermogravimetric analysis. To study the influence of oxygen on the thermal degradation of FP110 containing APA6, TGA measurements in nitrogen and synthetic air were carried out. The nitrogen atmosphere simulates regions with lower oxygen content such as areas below or inside of the flame. Synthetic air imitates phenomena on hot sample surfaces and around the surface of the flame. To minimize surface-area-to-volume-effects, for example, problems with oxygen availability,

DOI: 10.1002/fam

small samples (1 to 10 mg) were studied. Figure 5 shows the TGA results of fiber-free APA6 samples with 15 wt%, 25 wt% FP110 load, pure APA6, as well as FP110 alone. The TGA results for 5 and 10 wt% FP110 are similar.

The TGA measurements in nitrogen atmosphere present that both the FR and polymer matrix PA6 simultaneously decompose at temperatures around 280 ± 10 °C. Already at 375 °C, the mass loss observed for all APA6 samples is higher than 99 wt%. Pure FP110 shows also one decomposition step which takes place at around 345 °C. Measurements in synthetic air produce a completely different result, excluding the TGA curve of pure FP110, which is nearly the same. All APA6 samples have three main stages of mass loss. The first one is around 304 °C, corresponding to the decomposition in nitrogen, and the second and third are around 423 °C and 514 °C, belonging to thermally more stable polymer phases. An explanation of this two additional decomposition steps is the oxygen-induced production of char. In presence of FP110, the first and second mass losses are larger, while the third ones are smaller, and the produced residues are thermally more stable. For instance, the mass loss of pure APA6 is bigger than 99.5 wt% at 600 °C, while in presence of 25 wt % FP110, the residual mass is 3.9 wt% and still 2.4 wt% at 700 °C. According to these TGA results, it can be assumed that the flame retardancy of FP110 supports the char formation in APA6 in oxygen-rich atmospheres.

3.1.3. Limiting oxygen index test. The results obtained from the LOI test for fiber free and CFR APA6 sample sets are presented in Figure 6. The LOI value of pure fiber-free APA6 is around 22.0 o_2%, which is 12.2 o_2% lower than the LOI value of pure CFR APA6, which is a result of the reduced polymer content of one third in the CFR samples. The LOI maximum of the fiber free set is 22.8

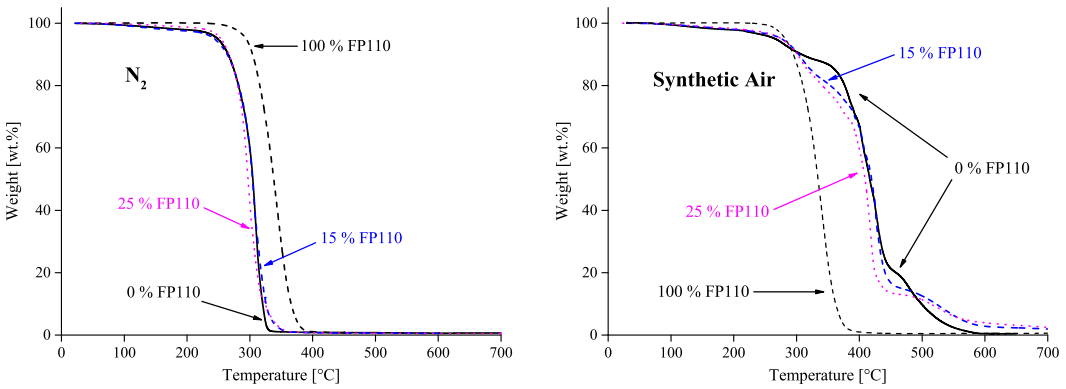

Figure 5. Thermogravimetric analysis results of fiber-free APA6 (left: nitrogen, right: synthetic air).

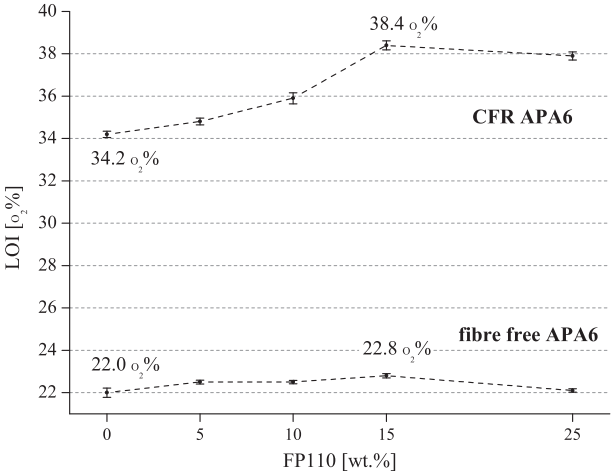

Figure 6. FP110-dependent limiting oxygen index values of fiber free and CFR APA6.

DOI: 10.1002/fam

o_2% in presence of 15 wt% FP110, while the measured LOI maximum of the CFR sets is 38.4 o_2%. The low effectiveness of FP110 in fiber-free APA6, wherein the LOI value increases only by 0.8 o_2%, is significantly increased by the fiber reinforcement — the maximum LOI increase in this case is 4.2 o_2%. Therefore, the fiber reinforcement has the highest influence of the flammability and the flame retardant efficiency of FP110 of APA6 composites. According to the cone calorimetry measurements, afterglow was observed for FR-free CFR APA6 samples, while both CFR-free and CFR-containing sample sets protected by FP110 exhibited strong charring. Char formation seems to be the main FR effect.

3.1.4. UL94 test. In the used vertical UL94 test method, vertically oriented samples were exposed to flame twice for 10 s. The achieved classification is based on both afterflame times, afterglow, and dripping. A V-0 is the best classification by UL94. The results of the UL94 test for CFR APA6 are shown in Table III.

All sample sets show no ignition after the first flame treatment. The average burning time after the second flame treatment decreases from 161 s (0 wt% FP110) over 114 s (5 wt% FP110) to 63 s (10 wt% FP110) with increasing FR loading. The sample sets with 15 wt% FP110 and 25 wt% FP110 are not ignited during both flame applications. These two sets achieve a V-0 classification. Because of the high fiber reinforcement, no melt flow or dripping is possible. According to the UL94 test results, CFR APA6 with at least 15 wt% FP110 shows sufficient flame retardancy.

3.1.5. FAR 25.853F1 test. Materials for application in an aircraft have to pass the FAR 25.853 test. Therefore, this test is essential for the produced CFR APA6 plates. The plates were tested according to the FAR 25.853, Appendix F (a)(1)(i)(vertical) test standard, which is suitable for interior compartments occupied by crew or passengers [74]. Figure 7 shows the test results. To pass the test, three criteria must be met: flame time lower than 15 s, burn length lower than 152.4 mm (6 inches), and the after flame time of a drip lower than 3 s.

Table III. UL94 results for CFR APA6.

FP110 [wt%]	Burning time [s]	UL94 classification
0	161	No classification
5	114	No classification
10	63	No classification
15	–	V-0
25	–	V-0

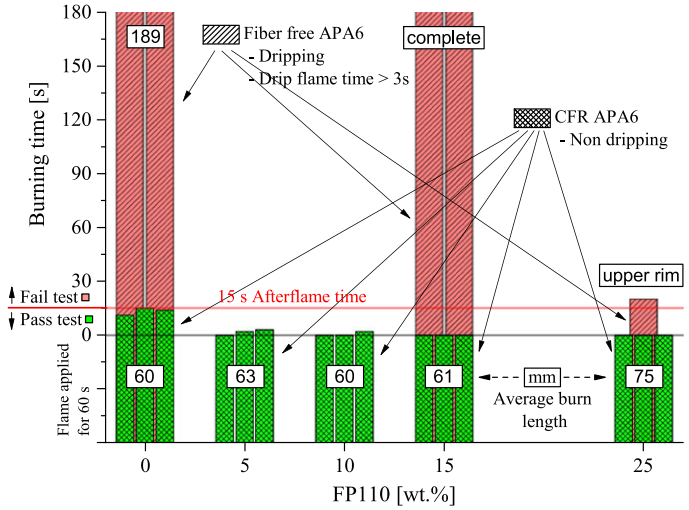

Figure 7. Federal Aviation Regulations 25.853F1 results for fiber free and CFR APA6.

DOI: 10.1002/fam

To estimate the FAR 25.853F1, the performance of FP110 in APA6 fiber-free plates with the highest FP110 loadings was tested. In this study, all tested fiber-free samples fail the test. Without FR, APA6 burns with a small flame and burning drops. In presence of FP110, the samples burn with a higher flame and with burning drops. The flame times of sample sets with 0 and 15 wt% FP110 loading are higher than 180 s. Both FP110 containing sets burn completely. The 25 wt% FP110 set burns only 20 s, but the whole sample surface is damaged by the flame. All tested CFR APA6 samples pass the FAR 25.853F1 test. Because of the UL94 results, we studied the area between 0 and 15 wt% and the highest possible FR content. Up to 10 wt% FP110, the sample sets still show short after burning times, but at higher loads, the flame goes out as soon as the burner flame is removed. The burned length for all sets is in the same area, and only the burned length of the 25 wt% set is slightly higher. Because of the fiber reinforcement, the samples are not dripping.

Based on the visual observation of the FAR 25.853F1 test, it was assumed that FP110 fire-protected APA6 shows higher char formation. FP110 free APA6 burns with a small flame at the bottom edge of the combusting polymer because the molten polymer flows away and drips from the sample. In case of fiber-free plates, the char increases the viscosity of the burning molten polymer. Dripping is made more difficult, whereby polymer pyrolysis is facilitated, and the observed flame grows. Because of the molten polymer surface, the char flows away and cannot form fire-protecting surfaces. Only the maximum FP110 load shows slightly better flame retardancy. In case of CFR plates, no dripping or polymer flow is observed. Therefore, the produced char is able to form stable fire-protecting surfaces. Already at 15 wt% FP110, no afterflame is recognized.

3.2. Mechanical properties

To evaluate the mechanical properties, the exact fiber content and the residual monomer content of each CFR plate were determined. In Table IV, the measured fiber contents of CFR APA6 plates are shown. Polymer matrix content (APA6 + FP110; in nitrogen atmosphere completely pyrolyzed; refer to Figure 5) and APA6 content of the polymer matrix are calculated from the measured fiber content. The fiber content in vol.% is calculated on the assumption that the density of resin mixture is 1.15 g/cm^3 and the density of the carbon fiber is 1.78 g/cm^3.

The fiber content of the CFR APA6 plates averages between 64 and 53 vol.%. No significant disturbing influence of the FR is observed. The fiber content deviations are located in the expected range caused by variations of plate thickness and weight of the carbon fabric. With increasing FR content, the fiber content near the ejector rises slightly, which means that the resin content decreases. A possible explanation for this observation is worse infiltration of the fabric caused by rising melt viscosity as a result of FP110 addition. The fiber content close to sprue is not influenced by FP110 content. The residual monomer content is displayed in Figure 8.

The content of residual ε-caprolactam increases with the FR loading. Till 15 wt% FP110, the residual monomer content is lower or equal to 1 wt%, also for PA6 recalculated results. Therefore, mechanical properties should not be influenced by the residual ε-caprolactam content.

Table IV. Fiber content of the CFR APA6 plates.

FP110 [wt%]	Sampling point near	Fiber content [wt%]	Fiber content [vol.%]	polymer matrix content [wt%]	APA6 content [wt%]
0	Sprue	63.5 ± 0.71	53.0 ± 0.77	37	37
	Ejector	63.0 ± 0.06	52.4 ± 0.06		
5	Sprue	62.2 ± 0.45	51.5 ± 0.48	37	35
	Ejector	63.2 ± 0.06	52.6 ± 0.06		
10	Sprue	64.3 ± 0.40	53.7 ± 0.43	36	32
	Ejector	64.4 ± 0.13	53.9 ± 0.14		
15	Sprue	63.7 ± 0.15	53.2 ± 0.16	36	30
	Ejector	65.0 ± 0.77	54.6 ± 0.84		
25	Sprue	63.7 ± 0.63	53.1 ± 0.67	35	27
	Ejector	65.5 ± 0.58	55.1 ± 0.63		

DOI: 10.1002/fam

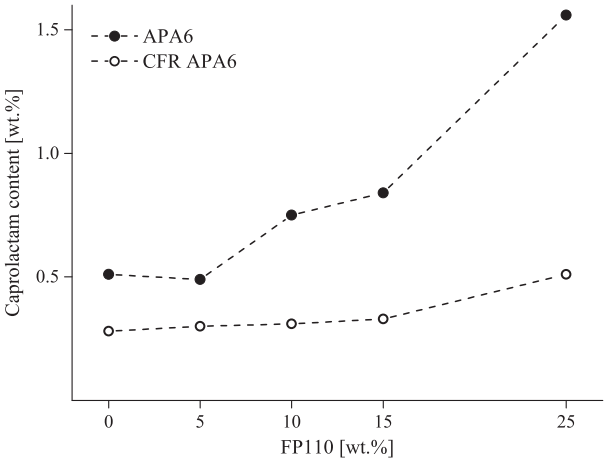

Figure 8. Residual monomer contents (ε-caprolactam) of APA6 plates.

3.2.1. Flexural test. In Figure 9, the flexural strength and E-modulus of CFR APA6 plates are shown. The flexural modulus increases (from 113.1 ± 2.0 GPa at 0 wt% FP110 to 123.6 ± 4.2 GPa 25 wt% FP110), and the flexural strength decreases (from 1440 ± 42 MPa at 0 wt% FP110 to 1035 ± 47 MPa at 25 wt% FP110) with increasing FP110 content. Consequently, the samples with high FR content are brittle and easy to break.

3.2.2. Compressive test. In Figure 10, the compressive strength and modulus of CFR APA6 plates are shown.

Both values decrease at higher FR loads. Accordingly, the FR weakens the mechanical stability of the polymeric matrix by a weakening of intermolecular interactions, such as the amidic hydrogen bonds. Along the fiber direction (0° fiber orientation), the values of both parameters are much higher (compressive strength: 3.7 to 3.9 times; compressive modulus: 12 to 15 times).

3.2.3. Tensile test. In Figure 11, the tensile strength and the Young's modulus of CFR APA6 plates are displayed. Both tensile strength and Young's modulus decrease at higher FR levels, with the exception of Young's modulus at 0° fiber orientation. These values are nearly equal. The results of both parameters are much higher at 0° fiber orientation (tensile strength: 24 to 37 times; Young's modulus: 14 to 21 times).

3.2.4. Charpy impact test. In Figure 12, the impact resistances of CFR APA6 plates are shown. The impact resistances rise from 90.4 ± 5.0 kJ/m^2 at 0 wt% FP110 to 107.9 ± 5.1 kJ/m^2 at 25 wt% FP110 with increasing FR content. FP110 accordingly acts as a positive impact modifier.

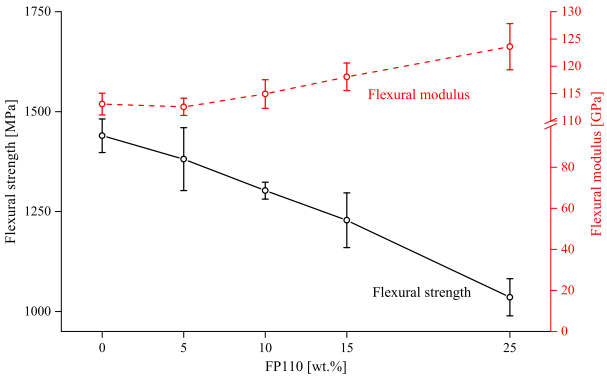

Figure 9. FP110-dependent flexural strength and modulus of CFR APA6.

DOI: 10.1002/fam

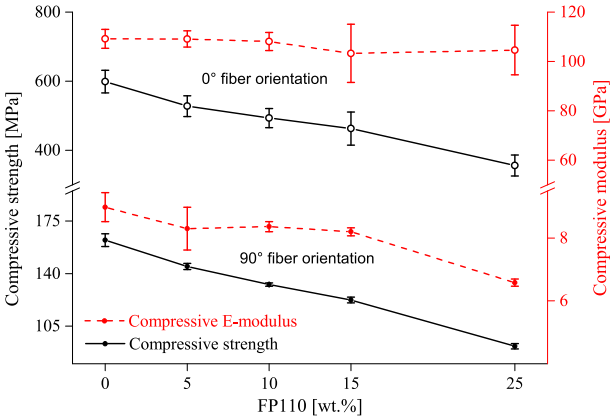

Figure 10. FP110-dependent compressive strength and modulus of CFR APA6.

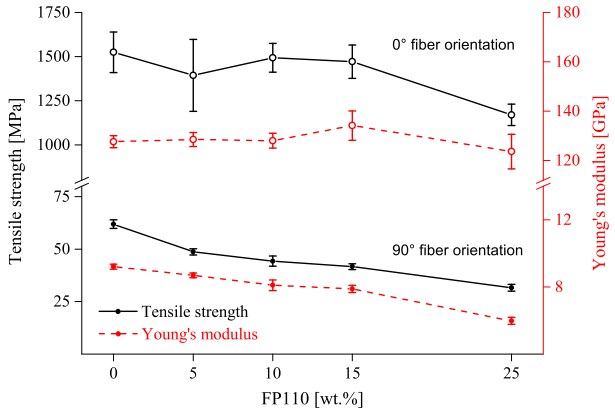

Figure 11. FP110-dependent tensile strength and Young's modulus of CFR APA6.

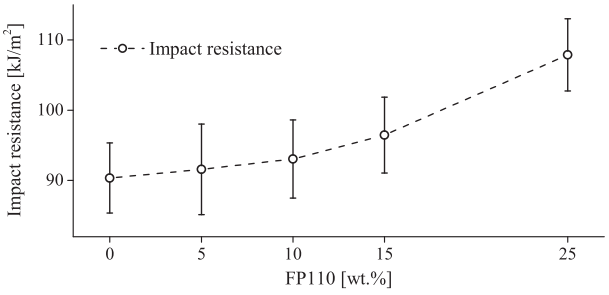

Figure 12. FP110-dependent impact resistance of CFR APA6.

3.2.4. DIFFERENTIAL SCANNING CALORIMETRY

In Figure 13 and Table V, the results of the DSC measurements are displayed. During the first heating process, all DSC curves with the exception of the 25% FP110 curve are very similar. Only the melting point of PA6 at approximately 215 to 219 °C is observed. The 25% FP110 sample shows further a signal around 105 °C, which is explainable by melting of the FP110. During the first cooling and second heating step, the peak positions in all curves are equal. The re-crystallization peak can be seen around 176 °C. During the second heating step, three significant regions are detected. First one is around 50 °C, which is a typical temperature region for the glass transition of PA6. The second

DOI: 10.1002/fam

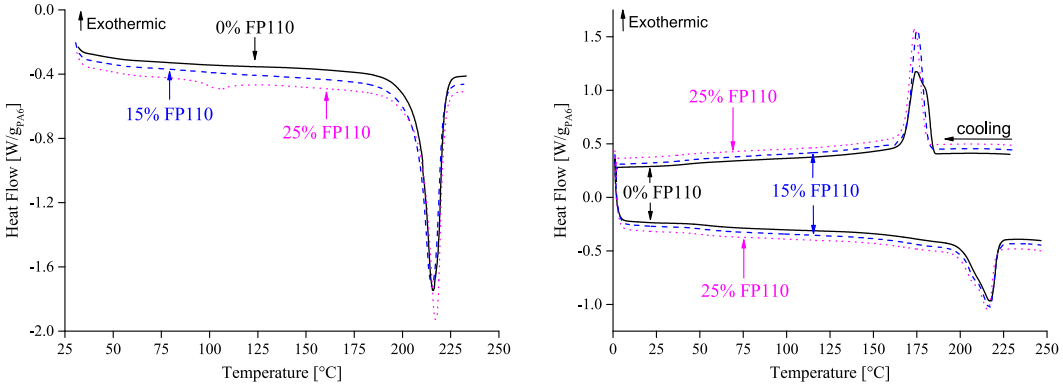

Figure 13. Differential scanning calorimetry curves of fiber-free APA6 plates (left: 1st heating; right: 1st cooling and 2nd heating).

Table V. DSC results of fiber free APA6 plates.

	1st heating			1st cooling and 2nd heating				
FP110 [wt%]	Melting point [°C]	ΔH_f [J/g$_{PA6}$]	Crystallinity [%]	Crystallization temperature [°C]	Melting point [°C]	ΔH_f [J/g$_{PA6}$]	Crystallinity [%]	Glass transition [°C]
0	216	90.8	39	175	217	59.9	26	54
5	216	90.2	39	175 180	217	60.0	26	52
10	219	92.9	40	177	217	62.0	27	50
15	215	90.7	39	175	217	61.6	27	49
25	105 217	4.5 89.9	– 39	174	216	56.6	25	48

and third ones are the region below the main signal at about 150 °C, and the other main signal is observed around 217 °C, which includes two overlapping peaks. For PA6 beside an amorphous phase, three major crystalline forms – a stable monoclinic α-form, a metastable pseudo-hexagonal β-form, and an unstable monoclinic γ-form – are known [75]. The α- and γ-forms can display a double-peak above 200 °C. The β-peak is often hardly to be distinguished from the amorphous state [76], but the region below the main signal is possibly caused by the β-form.

Differential scanning calorimetry (DSC) measurements can be used to characterize the crystallinity of semi-crystalline polymers like PA6 [77]. To calculate the degree of crystallinity, the determined heat of fusion (ΔH_f) applied to the PA6 content and a theoretical heat of fusion for 100% crystallinity (ΔH_f^o) are used [77]:

$$\text{Crystallinity} = \frac{\Delta H_f}{\Delta H_f^o} \cdot 100\%$$

For ΔH_f^o, the generally accepted average value (100% α-form) of 230 ± 20 J/g was used [77]. In Table V, the ΔH_f and calculated crystallinities are given. In both heating steps, the crystallinities are independent of the FR content. The crystallinity of T-RTM APA6 plates is about 40%.

In all DSC measurements, with the exception of the 25% FP110, no FP110 melting signals are included. This indicates that the FP110 is not distributed in crystalline form among the polymer matrix. Possible forms are as amorphous particles or molecular coordinated within the polymer matrix.

4. CONCLUSION

Out of the twelve tested commercial FRs, only FP110 is suitable for APA6 produced via T-RTM processing. CFR and fiber-free APA6 plates were prepared via the T-RTM method with FP110

DOI: 10.1002/fam

loads up to 25 wt%. The best FR effects in CFR APA6 are achieved with 15 wt% and higher FR loads. It is possible to pass FAR 25.853 and the UL94 test with V-0 classification.

According to TGA and cone calorimetry, char formation is the essential FR mechanism of FP110 in this system. FP110-free CFR sets fail FR tests as a result of afterglow. Char formation caused by FP110 prevents this. However, it should be mentioned that the incorporation of fiber fabrics (64 wt %) led to significant increase of flame resistance of the CFR APA6 composite, which was indicated by the LOI testing.

The mechanical properties are significantly influenced by the FP110. With rising FP110 amount, the impact resistance (positive impact modifier), flexural E-modulus, and residual monomer content increase, while tensile strength, flexural strength, and compressive E-modulus decrease. Semi-crystallinity of APA6 (40%), tensile E-modulus, and compressive strength are nearly unchanged. This indicates that the FP110 acts only as a passive filler in the polymer matrix and has near to no reinforcing interactions with the polymer. We assume that FP110 interrupt the polymer chain interactions (for example, strong hydrogen bonds between amid groups) like an interaction-free inert filler (six phenoxy groups shield the phosphazene core). Therefore, the resistance of the APA6 matrix against mechanical stress is reduced by these FP110-generated defects.

At a FP110 amount of 15 wt% (pass FAR 25.853 and UL94 V-0), the following mechanical properties are obtained for CFR APA6: flexural strength: 1228 MPa and E-modulus: 118 GPa, compressive strength: 463 MPa (0°) and E-modulus: 103 GPa (0°), tensile strength: 1471 MPa (0°) and E-modulus: 134 GPa (0°), and impact resistant: 96 kJ/m^2.

The flame retardancy of the FP110-modified CFR APA6 allows its use in aerospace applications. With the possibility of using different fibers and fiber layups, it should be possible to adapt the properties of the composites to the requirements of the application in future work.

ACKNOWLEDGEMENTS

For performing many of the presented measurements, we thank Konstantin Andreev (FhG-ICT Pfinztal) for tests with different FRs, Ute Schwarz (OMPG Rudolstadt-Schwarza) for cone calorimetry, Uwe Podwojewski (FhG-ICT Pfinztal) for flexural, compressive, and tensile strength as well as impact resistant measurements, Jasmin Aniol (FhG-ICT Pfinztal) for TGA, and Anja Kaiser (FhG-ICT Pfinztal) for TGA and DSC. We also thank Cahit Arik (FhG-ICT Pfinztal) and Felix Liermann (FhG-ICT Pfinztal) for performing the T-RTM process and Aleksandra Buczko (FhG-ICT Pfinztal) for her critical reading of this publication. Furthermore, we thank the Europeans and their EU project Clean Sky (Clean Sky Eco-Design, CSJU-GAM-ED-2009-001) for the financial support and Fushimi Pharmaceutical Co Ltd. and Nordmann, Rassmann for the material support of our work.

REFERENCES

1. Wiedmann M, Sinapius M. *Adaptive, Tolerant and Efficient Composite Structures*. Springer-Verlag: Berlin, 2013.
2. Soutis C. Carbon fiber reinforced plastics in aircraft construction. *Materials Science and Engineering A* 2005; **412**:171–176.
3. Drechsler K, Heine M, Mitschang P, Baur W, Gruber U, Fischer L, Öttinger O, Heidenreich B, Lützenburger N, Voggenreiter H. *Carbon Fiber Reinforced Composites*. Ullmann's Encyclopedia of Industrial Chemistry. Wiley-VCH: Weinheim, 2009.
4. Vodicka R. *Thermoplastics for Airframe Applications A Review of the Properties and Repair Methods for Thermoplastic Composites*. Aeronautical and Maritime Research Laboratory: Melbourne Victoria, 1996.
5. Hodzic A. Re-use, recycling and degradation of composites. In *Green Composites*, Baillie C (ed) chap. 12. Woodhead Publishing Limited: Cambridge, 2004; 252–271.
6. Ehrenstein GW, Kabelka J. *Reinforced Plastics*. Ullmann's Encyclopedia of Industrial Chemistry. Wiley-VCH: Weinheim, 2012.
7. Bitterlich M, Ehleben M, Wollny A, Desbois P, Renkl J, Schmidhuber S. Tailored to reactive polyamide 6. *Kunststoffe* 2014; **3**:47–51.
8. Reimschuessel HK. Nylon 6: Chemistry and Mechanisms. *Journal of Polymer Science: Macromolecular Reviews* 1977; **12**:65–139.
9. Weil ED, Levchik S. Current practice and recent commercial developments in flame retardancy of polyamides. *Journal of Fire Sciences* 2004; **22**:251–264.
10. Höhne CC. *Synergismus im Flammschutz*. Problemorientierte Projektarbeit: TUBAF and ICT, 2014.
11. Kiliaris P, Papaspyrides CD, Xalter R, Pfaendner R. Study on the properties of polyamide 6 blended with melamine polyphosphate and layered silicates. *Polymer Degradation and Stability* 2012; **97**:1215–1222.

DOI: 10.1002/fam

12. Tai Q, Yuen RKK, Yang W, Qiao Z, Song L, Hu Y. Iron-montmorillonite and zinc borate as synergistic agents in flame-retardant glass fiber reinforced polyamide 6 composites in combination with melamine polyphosphate. *Composites: Part A* 2012; **43**:415–422.
13. La Camera D, Kormelink H, Bozovic-Vukic J, Perez Y. WO 2013/175452 A1, 2013.
14. Ke C, Li J, Fang K, Zhu Q, Zhu J, Yan Q. Enhancement of a hyperbranched charring and foaming agent on flame retardancy of polyamide 6. *Polymers for Advanced Technologies* 2011; **22**:2237–2243.
15. Doğan M, Bayramlı E. The flame retardant effect of aluminum phosphinate in combination with zinc borate, borophosphate, and nanoclay in polyamide-6. *Fire and Materials* 2014; **38**:92–99.
16. Samyn F, Bourbigot S. Thermal decomposition of flame retarded formulations PA6/aluminum phosphinate/melamine polyphosphate/organomodified clay: Interactions between the constituents? *Polymer Degradation and Stability* 2012; **97**:2217–2230.
17. Levchik SV, Levchik GF, Balabanovich AI, Weil ED, Klatt M. Phosphorus oxynitride: a thermally stable fire retardant additive for polyamide 6 and poly(butylene terephthalate). *Die Angewandte Makromolekulare Chemie* 1999; **264**:48–55.
18. Staggs JEJ. Modeling thermal degradation of polymers by population balance methods. In *Fire Retardancy of Polymeric Materials*, Vol. **2** chap. 18, Wilkiw CA, Morgan AB (eds). CRC Press: Boca Raton, 2010; 479–508.
19. Andreev K, Käbisch B, JTI Clean Sky ECO Design WP 2.1.3.06, 2012.
20. Buczko A, Stelzig T, Bommer L, Rentsch D, Heneczkowski M, Gaan S. Bridged DOPO derivatives as flame retardants for PA6. *Polymer Degradation and Stability* 2014; **107**:158–165.
21. Allcock HR. *Phosphorus–Nitrogen Compounds*. Academic Press: New York, London, 1972.
22. Liebig J. Nachtrag der Redaction. *Annalen der Pharmacie* 1834; **11**:139–150.
23. Rose H. Ueber eine Verbindung des Phosphors mit dem Stickstoff. *Annalen der Pharmacie* 1834; **11**:129–139.
24. Allcock HR, Kugel RL. Synthesis of high polymeric alkoxy and aryloxyphosphonitriles. *Journal of the American Chemical Society* 1965; **87**:4216–4217.
25. Allcock HR, Kugel RL, Valan KJ. Phosphonitrilic compounds. VI. High molecular weight poly(a1koxy- and aryloxyphosphazenes. *Inorganic Chemistry* 1966; **5**:1709–1715.
26. Allcock HR, Kugel RL. Phosphonitrilic compounds. VII. High molecular weight poly(diaminophosphazenes). *Inorganic Chemistry* 1966; **5**:1716–1718.
27. Gleria M, Po R, Giannotta G, Fiocca L, Bertani R, Fambri L, Mantia FPL, Scaffaro R. Cyclophosphazenes as polymer modifiers. *Macromolecular Symposium* 2003; **196**:249–270.
28. Allcock HR. Polyphosphazene elastomers, gels, and other soft materials. *Soft Matter* 2012; **8**:7521–7532.
29. Gleria M, De Jaeger R. Polyphosphazenes: a review. *Topics in Current Chemistry* 2005; **250**:165–251.
30. Allcock HR. Generation of structural diversity in polyphosphazenes. *Applied Organometallic Chemistry* 2013; **27**:620–629.
31. Teasdale I, Brüggemann O. Polyphosphazenes: multifunctional, biodegradable vehicles for drug and gene delivery. *Polymers* 2013; **5**:161–187.
32. Allcock HR, Morozowich NL. Bioerodible polyphosphazenes and their medical potential. *Polymer Chemistry* 2012; **3**:578–590.
33. Allcock HR. Hybrids of hybrids: nano-scale combinations of polyphosphazenes with other materials. *Applied Organometallic Chemistry* 2010; **24**:600–607.
34. Deng M, Kumbar SG, Wan Y, Toti US, Allcock HR, Laurencin CT. Polyphosphazene polymers for tissue engineering: an analysis of material synthesis, characterization and applications. *Soft Matter* 2010; **6**:3119–3132.
35. Allcock HR. Recent developments in polyphosphazene materials science. *Current Opinion in Solid State and Materials Science* 2006; **10**:231–240.
36. Mark JE, Allcock HR, West R. *Inorganic Polymers*, Vol. **2**. Oxford University Press: New York, 2005.
37. Allen CW. The use of phosphazenes as fire resistant materials. *Journal of Fire Sciences* 1993; **11**:320–328.
38. Pan M, Huang R, Wang T, Huang D, Mu J, Zhang C. Preparation and properties of epoxy resin composites containing hexaphenoxycyclotriphosphazene. *High Performance Polymers* 2014; **26**:114–121.
39. Laszkiewicz B, Kotek R. Properties of poly(ethylene terephthalate) with p-bromophenoxycyclophosphazene blends. *Hungarian Journal of Industrial Chemistry* 1989; **17**:221–227.
40. Kurachi Y, Okuyama T, Oohasi T. Synthesis and properties of urethane foams having a N3P3 ring compound. *Journal of Materials Science* 1989; **24**:2761–2764.
41. Levchik GF, Grigoriev YV, Balabanovich AI, Levchik SV, Klatt M. Phosphorus–nitrogen containing fire retardants for poly(butylene terephthalate). *Polymer International* 2000; **49**:1095–1100.
42. Qian LJ, Ye LJ, Xu GZ, Liu J, Guo JQ. The non-halogen flame retardant epoxy resin based on a novel compound with phosphaphenanthrene and cyclotriphosphazene double functional groups. *Polymer Degradation and Stability* 2011; **96**:1118–1124.
43. Ding J, Shi W. Thermal degradation and flame retardancy of hexaacrylated/hexaethoxyl cyclophosphazene and their blends with epoxy acrylate. *Polymer Degradation and Stability* 2004; **84**:159–165.
44. Chen S, Zheng QK, Ye GD, Zheng GH. Fire-retardant properties of the viscose rayon containing alkoxycyclotriphosphazene. *Journal of Applied Polymer Science* 2006; **102**:698–702.
45. Wang PS, Chiu WY, Chen LW, Denq BL, Don TM, Chiu YS. Thermal degradation behavior and flammability of polyurethanes blended with poly(bispropoxyphosphazene). *Polymer Degradation and Stability* 1999; **66**:307–315.
46. Käbisch B, Fehrenbacher U, Kroke E. Hexamethoxycyclotriphosphazene as a flame retardant for polyurethane foams. *Fire and Materials* 2013; **38**:462–473.

DOI: 10.1002/fam

47. Allcock HR, Taylor JP. Phosphorylation of phosphazenes and its effects on thermal properties and fire retardant behavior. *Polymer Engineering and Science* . 2000; **40**: 1177–1189.
48. Zhang T, Du Z, Zou W, Li H, Zhang C. Hydroxyl-phosphazene-wrapped carbon nanotubes and its application in ethylene-vinyl acetate copolymer. *Journal of Applied Polymer Science* 2013; **130**:4245–4254.
49. Coggio WD, Schultz WJ, Ngo DC, Waid RD, Juvin-Pedretti VM. DE 69510518T2, 2000.
50. DeEdwardo AH, Zitomer F, Stackman RW, Kramer CE. US 4042561, 1977.
51. Urabe H, Ohyama H, Suzuki M. DE 60101646T2, 2004.
52. Brossas J, Clouet G, Knipper M. DE 3586322T2, 1993.
53. Yabuhara T, Tada Y, Nakano S, Kameshima T, Nishioka Y, Takase H. DE 60011058T2, 2005.
54. La Camera D, Kormelink H, Bozovic-Vukic J, Pérez Y. US 2013/0331478 A1, 2013.
55. Yabuhara T, Tada Y, Kameshima T, Nakano S, Nishioka Y, Takase H. DE 69907251T2, 2004.
56. Tada Y, Moriya N, Inoue T, Suzuki A, Koyama S. Preparation and properties of novel cyclophosphazenes containing cyanato groups. *Phosphorus, Sulfur, and Silicon* 2012; **187**:1555–1567.
57. Tada Y, Moriya N, Kanazawa M, Asanuma K, Suzuki A, Koyama S. Preparation and properties of novel oligo (phenylene oxide)-branched cyclophosphazenes. *Polymer Chemistry* 2012; **3**:2815–2824.
58. Dahiya JB, Kandola BK, Sitpalan A, Horrocks AR. Effects of nanoparticles on the flame retardancy of the ammonium sulphamate-dipentaerythritol flame-retardant system in polyamide 6. *Polymers for Advanced Technologies* 2013; **24**:398–406.
59. König A. WO 2012/152805 A1, 2012.
60. König A. US 2012/0289634 A1, 2012.
61. König A, Xue S, Uske K, Roth M. WO 2012/098185 A1, 2012.
62. König A, Xue S, Uske K, Roth M. US 2012/0190781 A1, 2012.
63. Meredith PL. US 4029634, 1977.
64. Urabe H, Ohyama H, Suzuki M. US 2002/0198295 A1, 2002.
65. Urabe H, Ohyama H, Suzuki M. EP 1160276 A1, 2001.
66. De Jaeger R, Mazzah A, Gengembre L, Frere M, Jama C, Milani R, Bertani R, Gleria M. Surface functionalization with phosphazenes. V. Surface modification of plasma-treated polyamide 6 with fluorinated alcohols and azobenzene derivatives through chlorinated phosphazene intermediates. *Journal of Applied Polymer Science* 2008; **108**:3191–3199.
67. Artner J, Ciesielski M, Ahlmann M, Walter O, Döring M, Perez RM, Altstädt V, Sandler JKW, Schartel B. A novel and effective synthetic approach to 9,10-dihydro-9-oxa-10-phosphaphenanthrene-10-oxide (DOPO) derivatives. *Phosphorus Sulfur* 2007; **182**:2131–2148.
68. Herzog B, Kohan MI, Mestemacher SA, Pagilagan RU, Redmond K. *Polyamides*. Ullmann's Encyclopedia of Industrial Chemistry. Wiley-VCH: Weinheim, 2013.
69. van Rijswijk K, Teuwen JJE, Bersee HEN, Beukers A. Textile fiber-reinforced anionic polyamide-6 composites. Part I: the vacuum infusion process. *Composites: Part A* 2009; **40**:1–10.
70. van Rijswijk K, Teuwen JJE, Bersee HEN, Beukers A. Textile fiber-reinforced anionic polyamide-6 composites. Part II: investigation on interfacial bond formation by short beam shear test. *Composites: Part A* 2009; **40**:1033–1043.
71. Parker D, Bussink J, van de Grampel HT, Wheatley GW, Dorf EU, Ostlinning E, Reinking K, Schubert F, Jünger O. *Polymers, High-Temperature*. Ullmann's Encyclopedia of Industrial Chemistry. Wiley-VCH: Weinheim, 2012.
72. Schartel B. Uses of fire tests in materials flammability development. In *Fire Retardancy of Polymeric Materials*, Vol. **2** chap. 15, Wilkiw CA, Morgan AB (eds). CRC Press: Boca Raton, 2010; 387–420.
73. Allcock HR, McDonnell GS, Riding GH, Manners I. Influence of different organic side groups on the thermal behavior of polyphosphazenes: random chain cleavage, depolymerization, and pyrolytic cross-linking. *Chemistry of Materials* 1990; **2**:425–432.
74. FAA. FARs, part 25, appendix F1, sec. 25.853, 2003.
75. Klata E, Borysiak S, Van. de Velde K, Garbarczyk J, Krucińska I. Crystallinity of polyamide-6 matrix in glass fibre/polyamide-6 composites manufactured from hybrid yarns. *Fibres & Textiles in Eastern Europe* 2004; **12**:64–69.
76. Seguela R. On the strain-induced crystalline phase changes in semi-crystalline polymers: mechanisms and incidence on the mechanical properties. *Journal of Macromolecular Science Polymer Reviews* 2005; **45**:263–287.
77. Khanna YP, Kuhn WP. Measurement of crystalline index in nylons by DSC: complexities and recommendations. *Journal of Polymer Science, Part B: Polymer Physics* 1997; **35**:2219–2231.

DOI: 10.1002/fam